Eddy current septum magnets for injection and extraction at SSRF

OUYANG Lian-Hua(欧阳联华)[1)] GU Ming(谷鸣) LIU Bo(刘波) CHEN Rong(陈嵘)

Shanghai Synchrotron Radiction Facility, Shanghai 201203, China

Abstract There are 6 in-vacuum eddy current septum magnets used for booster injection, extraction, and storage ring injection in SSRF. Special attention was paid to coils and their support designs because of the shock force they bear in the magnetic fields and the high heat which is hard to be dissipated in vacuum environment. For the storage ring magnets, good transverse homogeneity in the gap was achieved by careful design, precise machining and accurate assembly; and an extremely low leakage field on the stored beam is another key feature thanks to the high permeability Mu metal. Magnetic field measurement was conducted with both a point coil and a long integral coil, and the results agree well with the OPERA-2d/3d simulations. An inner tube is added to keep the continuity of impedance for the circulating beam with two RF finger flanges at each end. There is no vacuum separation between the inner tube and the magnet chamber. Sputter ion pumps integrated with NEG are used to acquire the UHV for the chamber.

Key words injection and extraction, eddy current, septum magnets, leakage field

PACS 29.27.Ac

1 Introduction

The Shanghai Synchrotron Radiation Facility (SSRF), currently in commissioning stage, is a third generation light source. It consists of a linac, a booster and a storage ring with double bend achromatic (DBA) lattices and 432 m in circumference. The stored beam current will be 200–300 mA, with an energy of 3.5 GeV and an emittance of 3.9 nm·rad.

When the beam current with an energy of 150 MeV from the linac arrives at the end of the LTB transfer line, it will first be deflected by the septum magnet, then kicked onto the booster orbit by the kicker. After the energy is ramped to 3.5 GeV, the beam is extracted by a fast single turn extraction scheme which consists of one kicker, 3 slow kickers (bump magnets), one thin septum magnet and two thick septum magnets.

The injection into the storage ring will be in the horizontal plane by means of two septum magnets and four kickers. This method provides a smooth and continuous injection. The injection efficiency is the main concern of the septum magnets. To this end we rely on good transverse homogeneity in the gap for the injected beam and low leakage field on the circulating beam. Table 1 shows the basic parameters of some of the SSRF septum magnets.

Table 1. Basic parameters of booster thick septum magnets and storage ring septum magnets.

parameter name	booster extraction (thick)	storage ring injection
No. of magnets	2	2
length/m	0.6	0.8
deflection angle/mrad	52.20	55
magnetic field/T	1.015	0.8082
gap height and width/mm	12×40	12×40
minimum septum thickness/mm		$<3^*$
good field region/(mm·mm)	26×10	28×10
half sine pulse width/μs	60	60
repetition rate/Hz	2	2
field transverse homogeneity		2%
leakage field		0.1%

$*$ at injection point.

Received 23 March 2009

1) E-mail: fouyang2002@yahoo.com

2 Magnets design and vacuum considerations

Only the booster extraction thick septum magnet and the storage injection thin septum magnet are described below. The magnetic cores were laminated with steel sheets punched into U shape with a gap height of 12 mm and the width of 40 mm. The sheet material (10JNEX900) is non-oriented, double coated, 0.1 mm thick, with a high content of silicon. It has a low core loss and high permeability at high frequencies. The core was enclosed by OFHC copper box. Except the ends, all sides of the box were curved into arc shapes with different radii of curvature for booster magnet and storage magnet respectively. Eddy current will be induced in the septum wall at the outer side of the gap. The stray field out of the gap is largely cancelled by the effect of the eddy current. For the storage ring injection thin septum magnet, the thickness of the septum wall was optimized at less than 3 mm at the injection point. A trapezoidal trough was cut in the septum wall along the circulating beam direction, with the minimum thickness at the end of the injection point.

Both the booster extraction septum magnets and the storage ring injection septum magnets were placed in cylinder vacuum chambers. For the storage ring, it is of great importance to preserve the continuity of beam impedance, so an inner tube was added against the trapezoidal trough of the septum wall for the circulating beam (Fig. 1). Both its ends were connected with the RF fingers bellows to the other vacuum chamber of the storage ring injection straight section. There was no vacuum separation between the inner tube and the magnet chamber. Though the space at the injection point was very tight, a Mumetal sheet of 0.25 mm thick adapted to the outer surface geometry of inner tube forms a shielding screen to further reduce the leakage field.

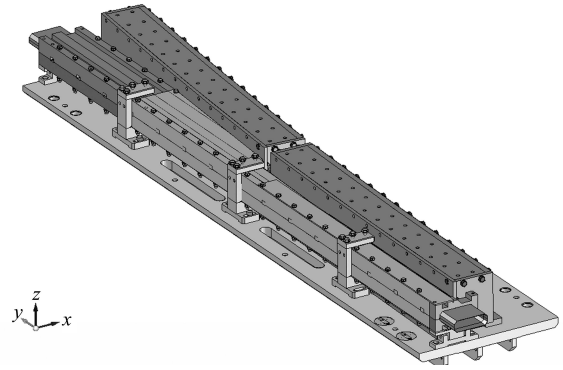

Fig. 1. View of the septum magnets with inner beam tube.

Because of the huge outgassing surfaces of the core sheets and the gas entrapment in each magnet, UHV treatments of all materials before the assembly and at least 200 ℃, 24 h baking before and after installation are necessary. For the booster magnet chamber, it needs a vacuum pressure of 5×10^{-6} Pa, which was acquired by using two 400 l/s sputter ion pumps. While for the storage ring one, it has a higher vacuum pressure (2.6×10^{-8} Pa), so three 400 l/s sputter ion pumps, each integrated with a 400 l/s SAES ST707 nonevaporable getter (NEG) were used.

3 Coil deformation and thermal analysis

The coil was made of solid copper bar, and wound around the back side of the core; its fixation and insulation made use of the machinable ceramic cut into suitable shape and placed in between the steel sheets as spacers to clamp firmly the coil.

For the booster extraction magnet, the deflection magnetic field is around 1.0 T, with gap height $g = 12$ mm, magnetic core length $L = 600$ mm, the peak value of magnetic force for a 2 Hz 60 μs half sine pulse on the coil is

$$|\boldsymbol{F}| = \int jB\mathrm{d}v = B_0^2 gL/2\mu_0 = 2865\,(\mathrm{N}), \qquad (1)$$

which agrees well with the result of OPERA-2d calculation

$$F_x = 2L\int L_x \mathrm{d}x\mathrm{d}y = 2649.2\,(\mathrm{N}). \qquad (2)$$

This is approximately equal to a pressure of 400000 $\mathrm{N/m^2}$ on the coil in the aperture. The force is on the horizontal plane, and the direction is to the inner side of the gap.

ANSYS LS-DYNA explicit finite element program was used for the dynamic analysis of coil deformation. The stress-strain relation is described by the bilinear isotropic plasticity model. For copper, the modulus of elasticity is 1.38×10^{11} $\mathrm{N/m^2}$, the Poisson's ratio 0.36, the yield stress 8.9×10^{7} $\mathrm{N/m^2}$, and the tangent modulus 1.28×10^{9} $\mathrm{N/m^2}$.

Two cases will be discussed here. The first has a section of 4 mm×8 mm and 5 pairs of ceramic spacers to clamp the coil. The results show there is a delay of displacement compared with the force pulse. At t=30 μs when the force reaches its peak, the maximum deformation is 3.2 μm; at t=2000 μs, the maximum deformation is 0.67 mm. Most of it is elastic, only a small part is plastic (about 15 μm) (Fig. 2(a)).

But on a month and longer time basis, the deformation accumulation is big, enough to cause a short with the core if no other measure will be taken.

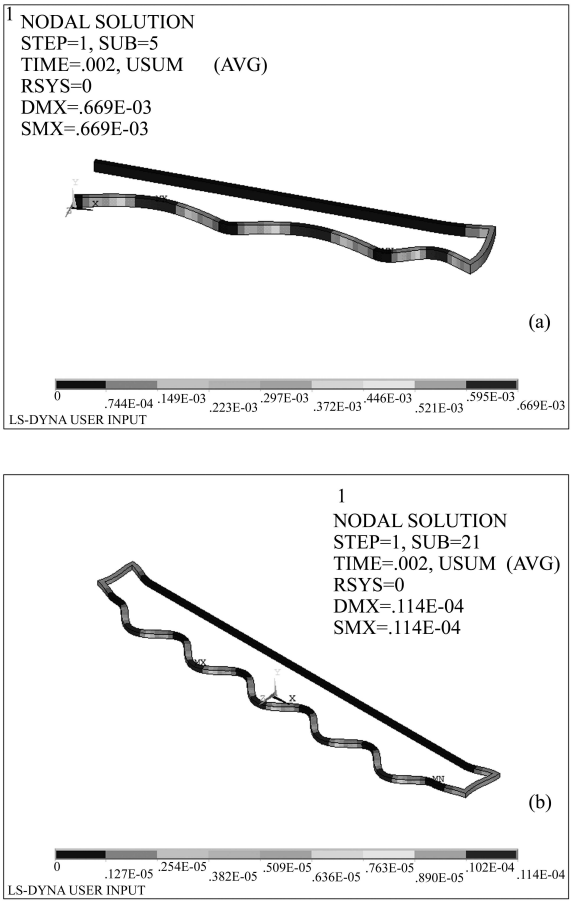

Fig. 2. Deformation for a coil of section of 4 mm×8 mm (a), and 6 mm×6 mm (b).

The second case is the section of 6 mm×6 mm and 6 pairs of ceramic spacers. At t=2 ms, the maximum deformation is 11 μm, and it is totally elastic, that is, there is no deformation when the force is removed (Fig. 2(b)).

The ANSYS electric and thermal coupling analysis was carried out for the coil. Because of the skin effect (the skin depth is 0.7 mm), the resistance of the coil with a section area of 32 mm^2 and a length 1400 mm is 1.64 mΩ. Given a 5 mΩ contact resistance for the copper braid which connects the coil and the feedthrough, and a 79 A current for the load (rms value of 2 Hz, 60 μs half sine with amplitude of 10200 A), the joule heat generation is 4.84×10^7 W/m^3.

The thermal conductivity of the copper coil changes from 401 W/(m·K) to 366 W/(m·K) when the temperature changes from 27 ℃ to 527 ℃; Its specific heat changes from 385 J/(kg·K) to 417 J/(kg·K) when the temperature changes from 25 ℃ to 327 ℃; For ceramic, the conductivity and specific heat are not temperature dependent, and the values are 1.46 W/(m·K) and 790 J/(kg·K) respectively.

Since there is no convection in the UHV environment, and the radiation is negligible, most of the heat in the coil is dissipated to the air through the feedthrough and vacuum chamber. For the boundary condition, two assumptions are given. The first one is the temperature for the part of feedthrough in the air to be fixed to 45 ℃; the second is that in addition to the first condition, the temperature for the ceramic sides which contact the magnet copper box be fixed to 100 ℃.

Figure 3 shows the temperature distribution of the coil on the two assumptions. The maximum temperature is about 198 ℃, and the minimum 134 ℃. In fact, the real temperature is somewhere in between them.

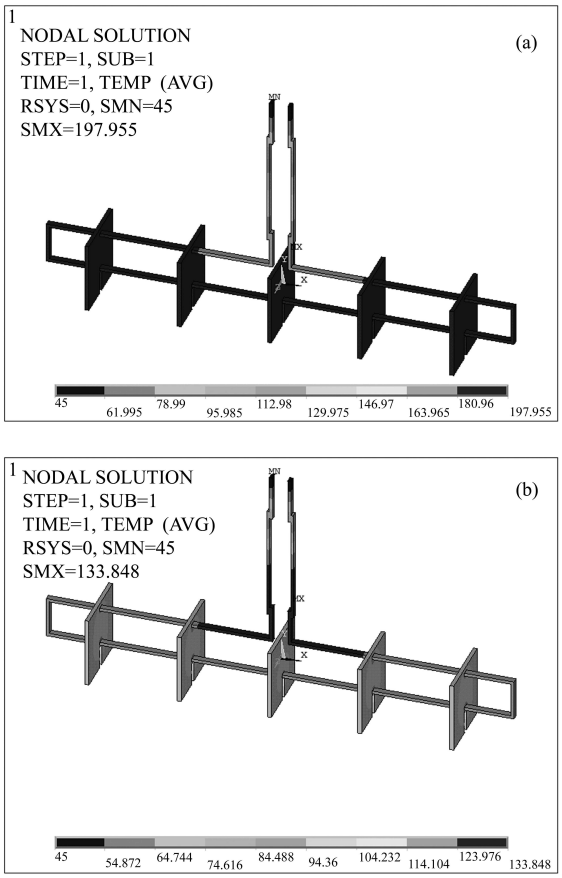

Fig. 3. Temperature distribution of the coil on the first assumption (a) and the second assumption (b).

4 Magnetic field analysis

Nonlinear transient eddy-current electromagnetic field analysis was performed on the septum magnets

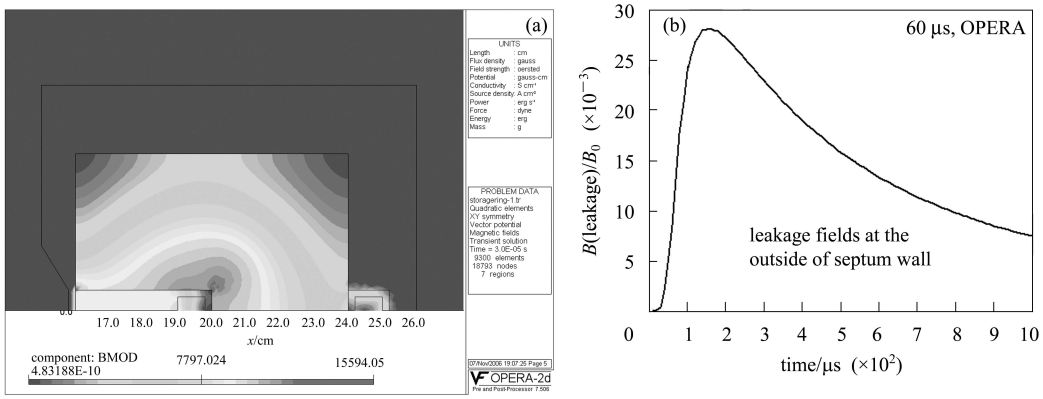

Fig. 4. 2D field distribution.

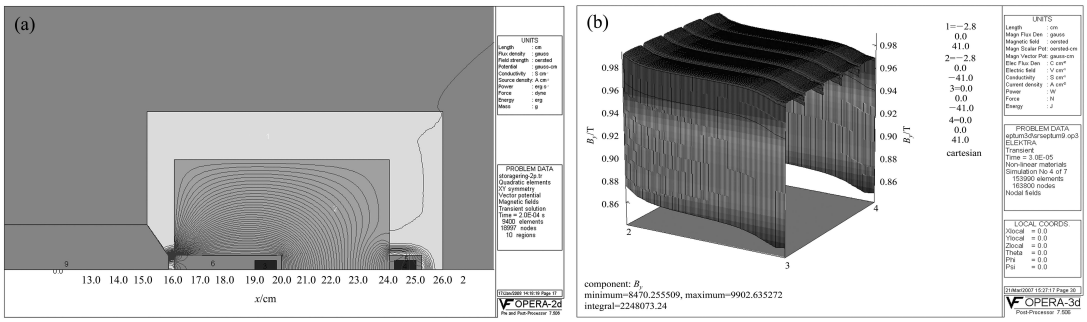

Fig. 5. The magnetic flux distribution for the 2D model with Mumetal shielding screen (a), and results of 3D simulation (b).

using Opera-2D and Opera-3D (ELEKTRA).

Figure 4 shows the 2D field distribution at pulse peak when t=30 μs (a) and the time evolution of the leakage field (b). The main field transverse homogeneity is about ±3.3‰; and one can notice that there is a time delay between the main field and the leakage field which reaches its peak at $t \approx 150$ μs. The ratio to the main field is around 2.8%.

Figure 5 shows the magnetic flux distribution at t=200 μs for the 2D model with the Mumetal shielding screen adapted to the inner beam tube geometry (a) and the main field at the median plane of the 3D simulation (b). One can notice that at the positions of the ceramic spacers the values of the magnetic fields have a slight drop. Since these drops occur in the longitudinal direction, they don't affect the beam deflection transversely [1].

5 Magnetic measurement

The magnetic field measurement was performed on each of the septum magnets for transverse homogeneity, longitudinal profile, effective magnetic length, and integral leakage field versus distance from the septum wall. The measuring equipment consists of:

1) "point" coil (4 mm in diameter, 20 turns), long coil of 6 mm wide;

2) Integrator (home made);

3) Agilent 54810A or LeCroy Wavesurfer 42XS digital integrator oscilloscope Current transformer, and

4) ulsed power supply

The following are the results for storage ring injection septum magnets. Fig. 6 shows the longitudinal profile of peak values of local main field (a), and time profile of integrated main field (b). From these data we can calculate that the effective magnetic length is 801.45 mm, and the transverse homogeneity of 0.4% for x=2–16 mm ($x = 0$ is the position of septum inner surface).

Leakage field measurement was performed first on a prototype magnet without Mumetal shielding screens. The peak values of leakage field versus distance from the septum wall are shown in Fig. 7.

Then the measurement was performed on the storage ring injection septum magnets with Mumetal shielding screens. Amazingly any effective leakage

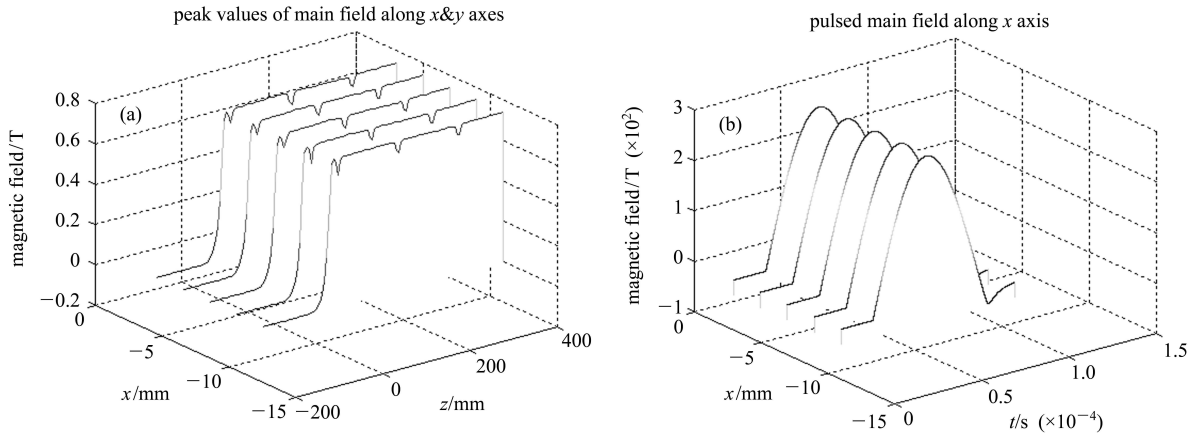

Fig. 6. Longitudinal profile of peak values of magnetic field (a) and main field integral profile (b).

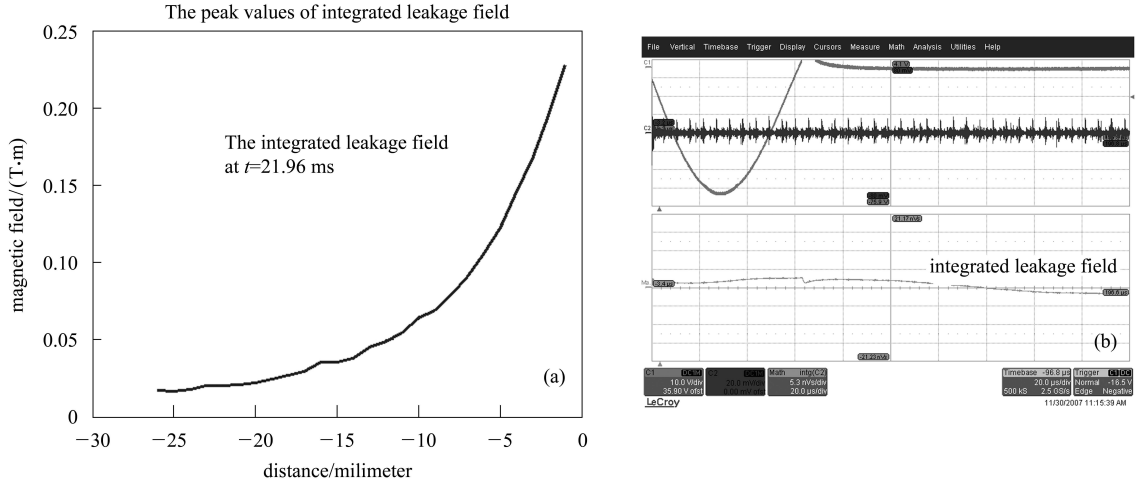

Fig. 7. The peak values of leakage field versus distance from the septum wall.

field signal cannot be seen at all in the precision range of the LeCroy Wavesurfer 42XS digital integrator oscilloscope. It is safe to say the ratio of integrated leakage field to integrated main field is less than 0.005% [2].

6 Conclusion

All six in-vacuum eddy current septum magnets were designed, manufactured, tested, and installed in SSRF. In addition to the work mentioned above, the magnets position adjustment and alignment were also key procedures to ensure their good performance. High stability and reliability were as important as the characteristics such as good integrated main field transverse homogeneity and extremely low leakage field on the stored beam. The connection and fixation of the coil to the pulse power supply is something which requires more attention and care. The high injection efficiency in beam commissioning demonstrates that all six septum magnets have achieved their design goals despite the many engineering challenges.

References

1 KANG Wen, HAN Qian, FU Lu-Xin et al. Development of an Eddy-current Septum Magnet for the SSRF Storage Ring. APAC 2001 Proceedings. Beijing China, 2001. 663–665

2 Gough C, Mailand M. Septum and Kicker Systems for the SLS. PAC 2001 Proceedings. Chicago, US, 2001, **5**: 3741–3743